Supporting Information for

Cancer stem cell activity of copper(II)-terpyridine complexes with sulfonamide groups

Karampal Singh, [a†] Joshua Northcote-Smith,[a†] Kuldip Singh, [a] and Kogularamanan Suntharaligam [a*]

[a] School of Chemistry, University of Leicester, Leicester, LE1 7RH, United Kingdom;
[†] These authors contributed equally to this work

* To whom correspondence should be addressed:
Email: k.suntharalingam@leicester.ac.uk

Table of Content

Reference

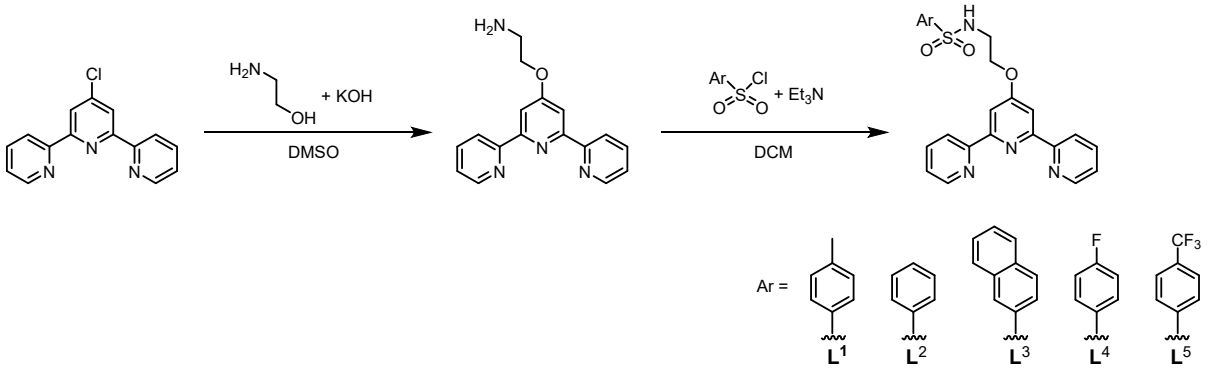

Figure S1. The reaction scheme for the preparation of terpyridine ligands containing various aryl sulfonamide groups $\mathbf{L^1}$-$\mathbf{L^5}$.

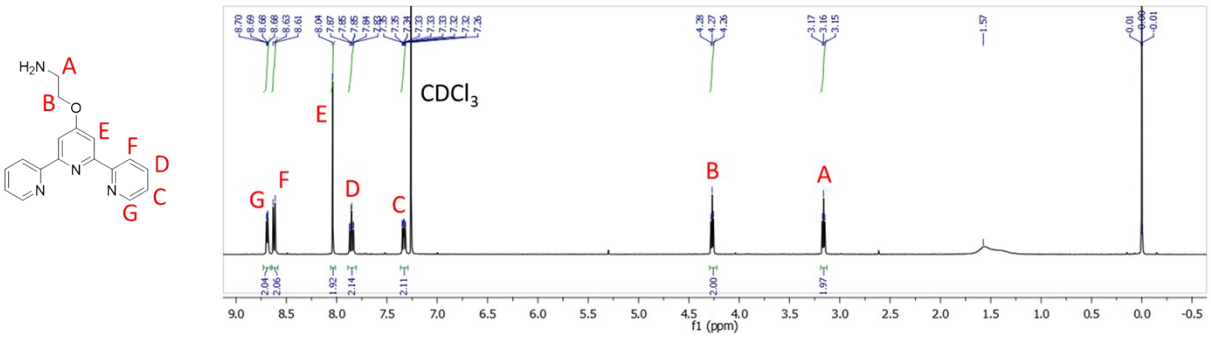

Figure S2. ^{1}H NMR spectrum of 2-([2,2':6',2"-terpyridin]-4'-yloxy)ethan-1-amine in $CDCl_3$.

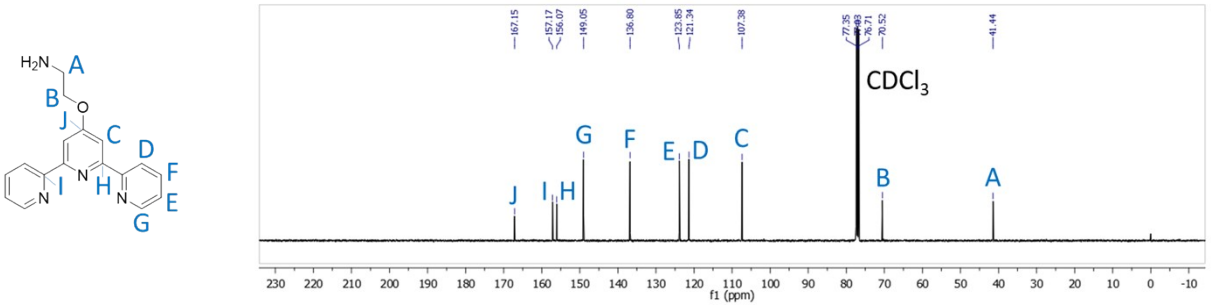

Figure S3. $^{13}C\{^1H\}$ NMR spectrum of 2-([2,2':6',2"-terpyridin]-4'-yloxy)ethan-1-amine in $CDCl_3$.

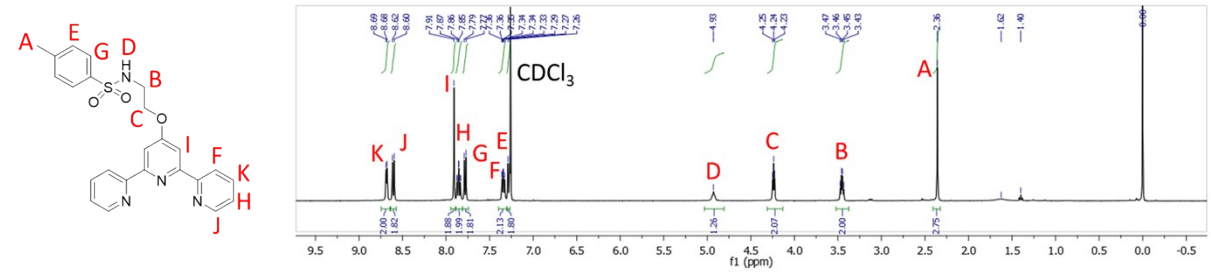

Figure S4. ^{1}H NMR spectrum of $\mathbf{L^1}$ in $CDCl_3$.

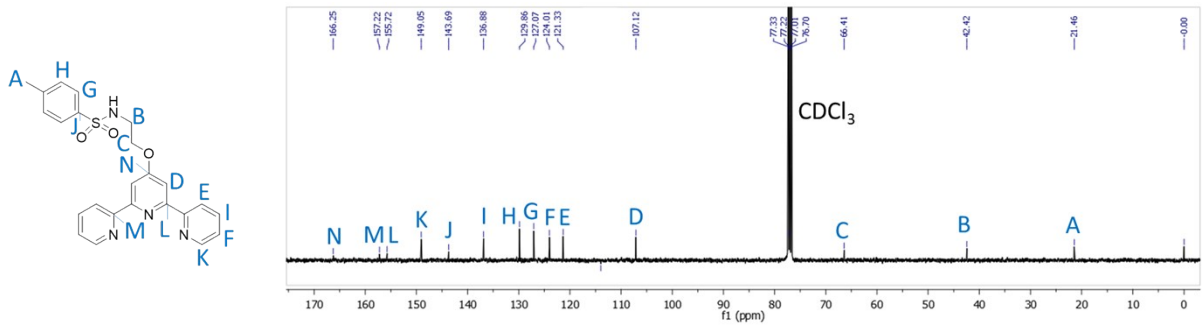

Figure S5. $^{13}C\{^{1}H\}$ NMR spectrum of $\mathbf{L^1}$ in $CDCl_3$.

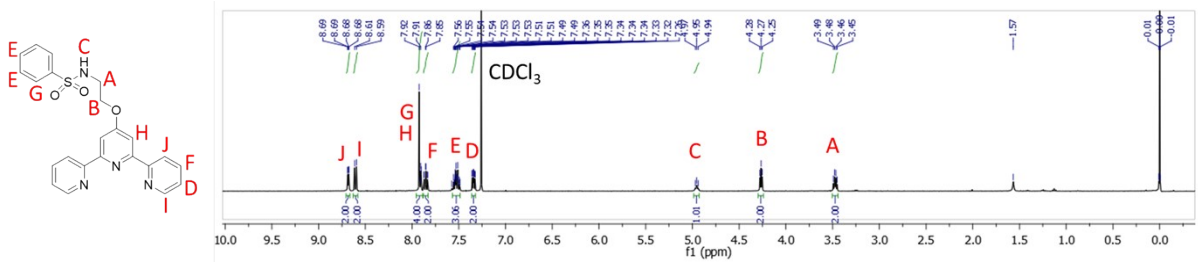

Figure S6. ^{1}H NMR spectrum of $\mathbf{L^2}$ in $CDCl_3$.

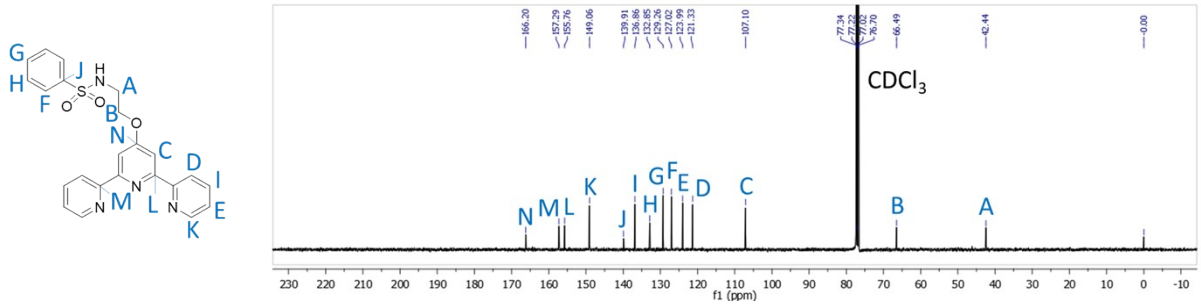

Figure S7. $^{13}C\{^{1}H\}$ NMR spectrum of $\mathbf{L^2}$ in $CDCl_3$.

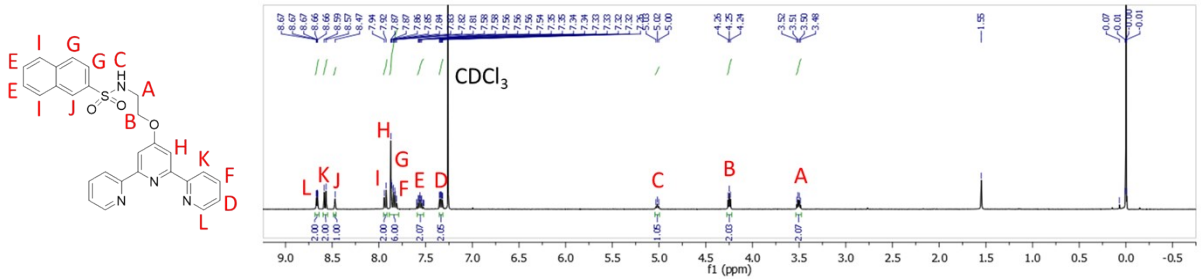

Figure S8. ^{1}H NMR spectrum of $\mathbf{L^3}$ in $CDCl_3$.

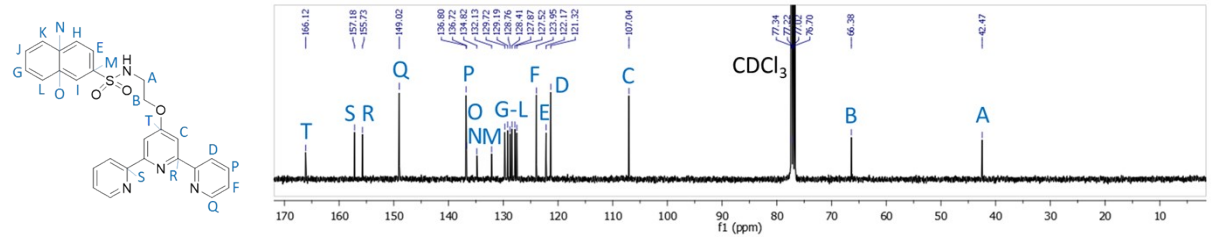

Figure S9. $^{13}C\{^{1}H\}$ NMR spectrum of **L³** in $CDCl_3$.

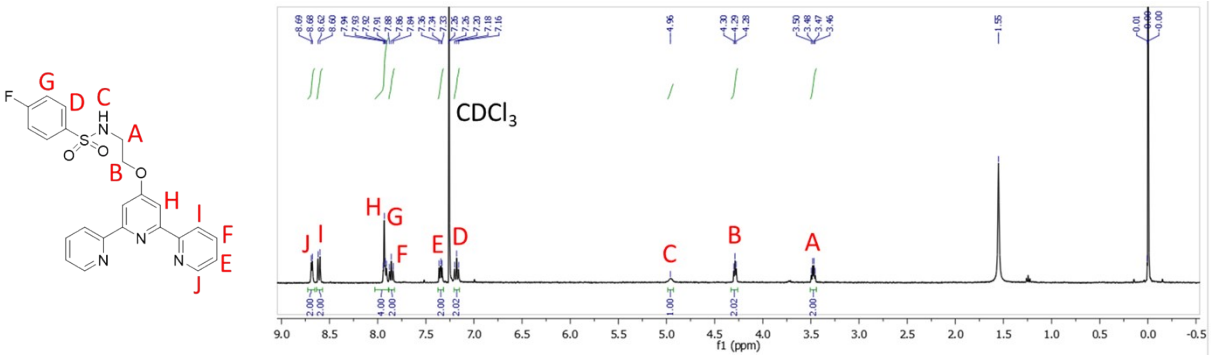

Figure S10. ^{1}H NMR spectrum of **L⁴** in $CDCl_3$.

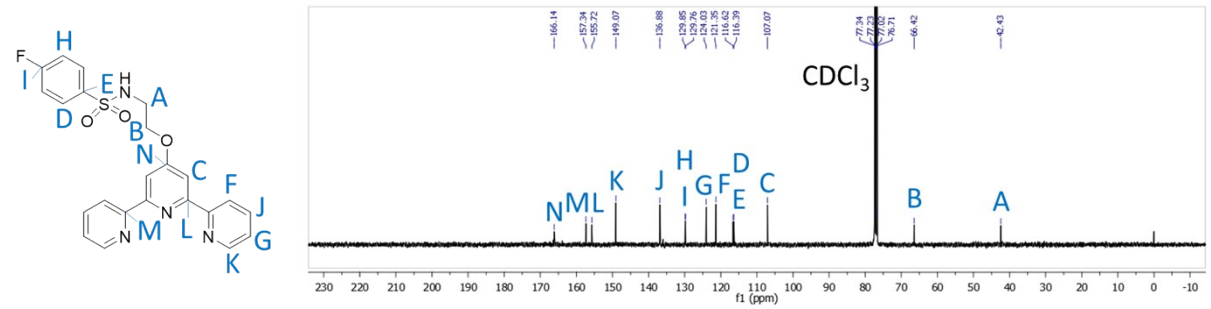

Figure S11. $^{13}C\{^{1}H\}$ NMR spectrum of **L⁴** in $CDCl_3$.

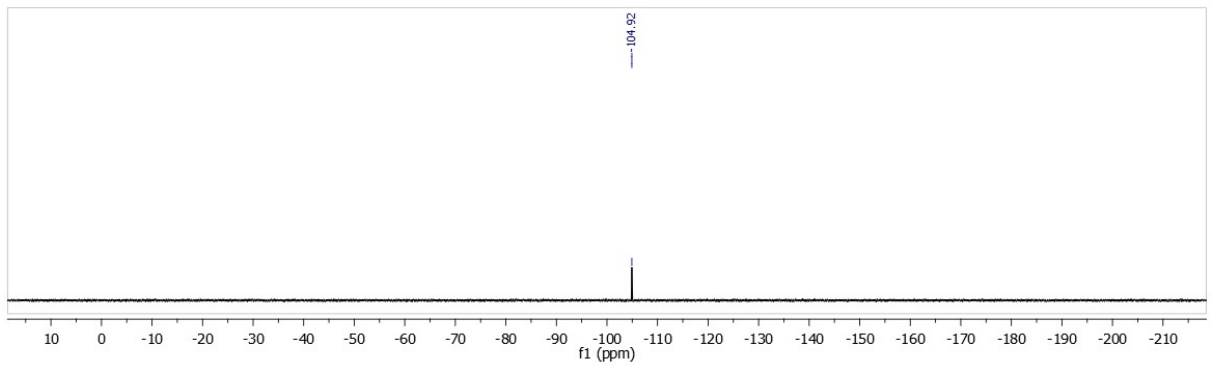

Figure S12. $^{19}F\{^{1}H\}$ NMR spectrum of **L⁴** in $CDCl_3$.

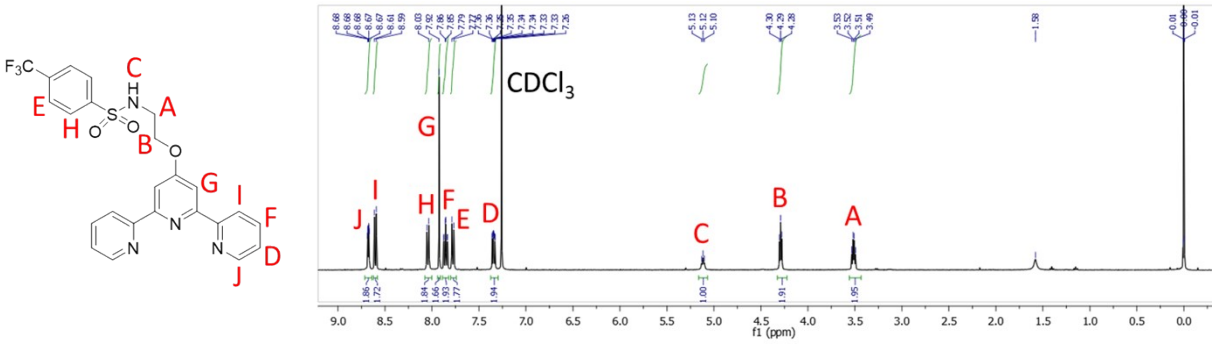

Figure S13. ^{1}H NMR spectrum of **L^{5}** in $CDCl_3$.

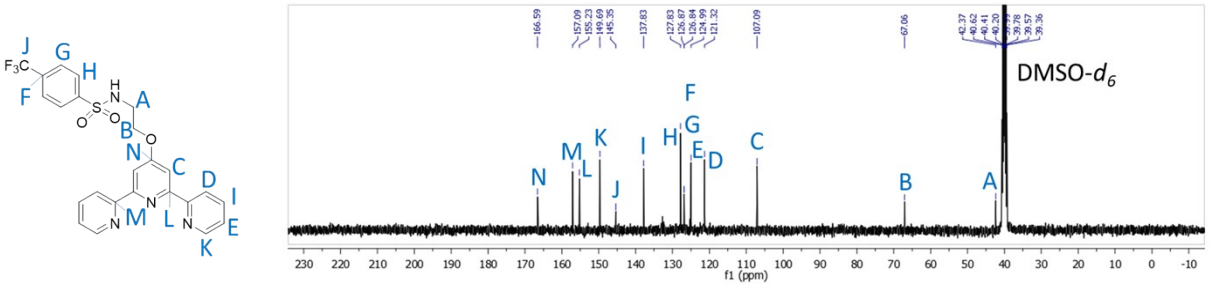

Figure S14. ^{13}C{^{1}H} NMR spectrum of **L^{5}** in DMSO-d_6.

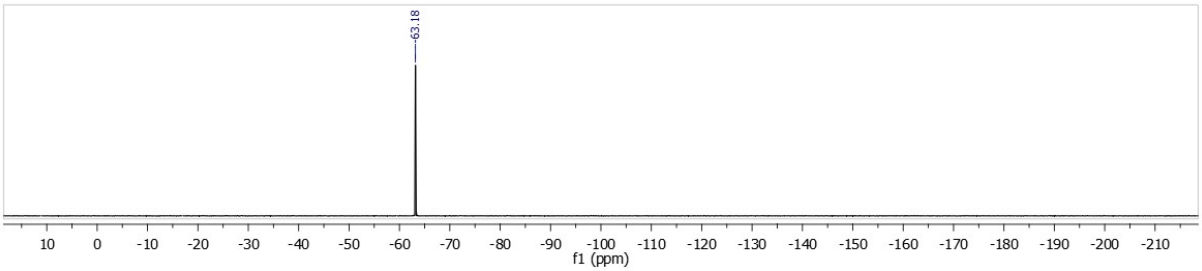

Figure S15. ^{19}F{^{1}H} NMR spectrum of **L^{5}** in $CDCl_3$.

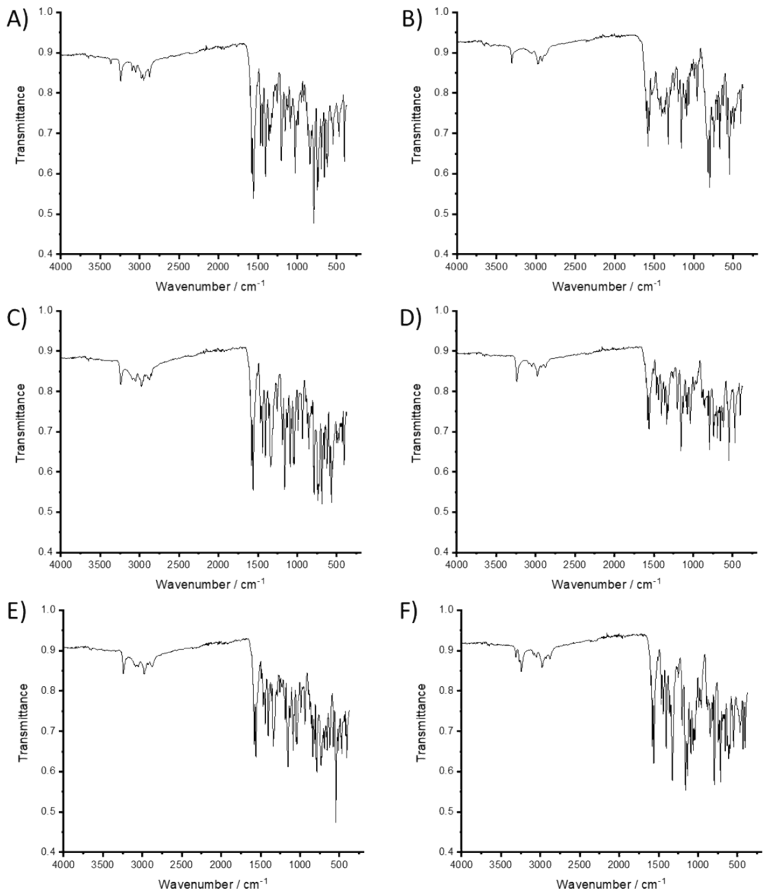

Figure S16. ATR-FTIR spectra of (A) 2-([2,2':6',2"-terpyridin]-4'-yloxy)ethan-1-amine, (B) **L**[1], (C) **L**[2], (D) **L**[3], (E) **L**[4], (F) **L**[5] in the solid form.

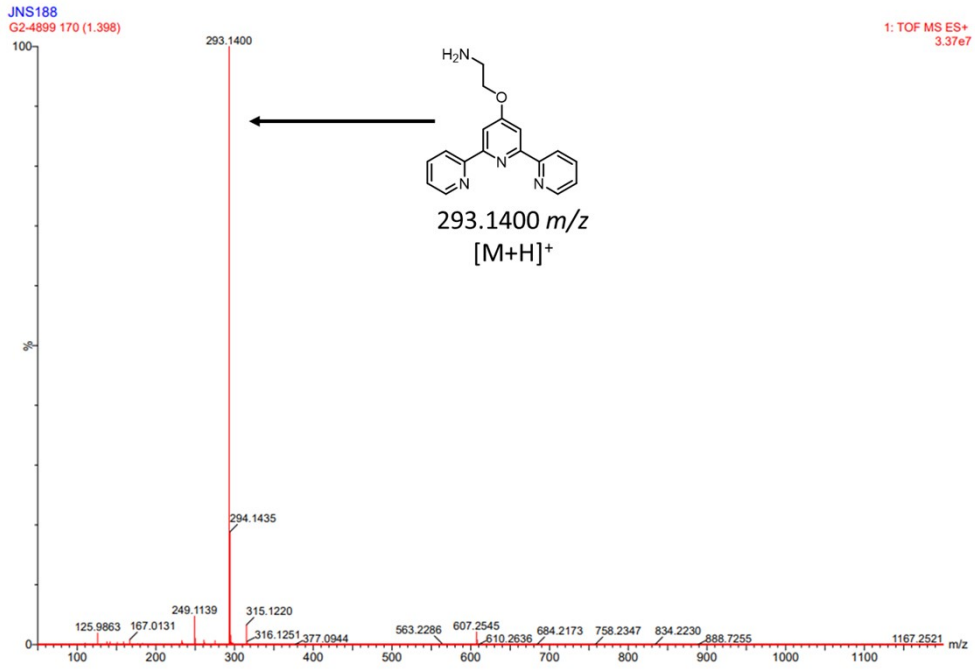

Figure S17. High-resolution ESI-MS mass spectrum (positive mode) of 2-([2,2':6',2"-terpyridin]-4'-yloxy)ethan-1-amine.

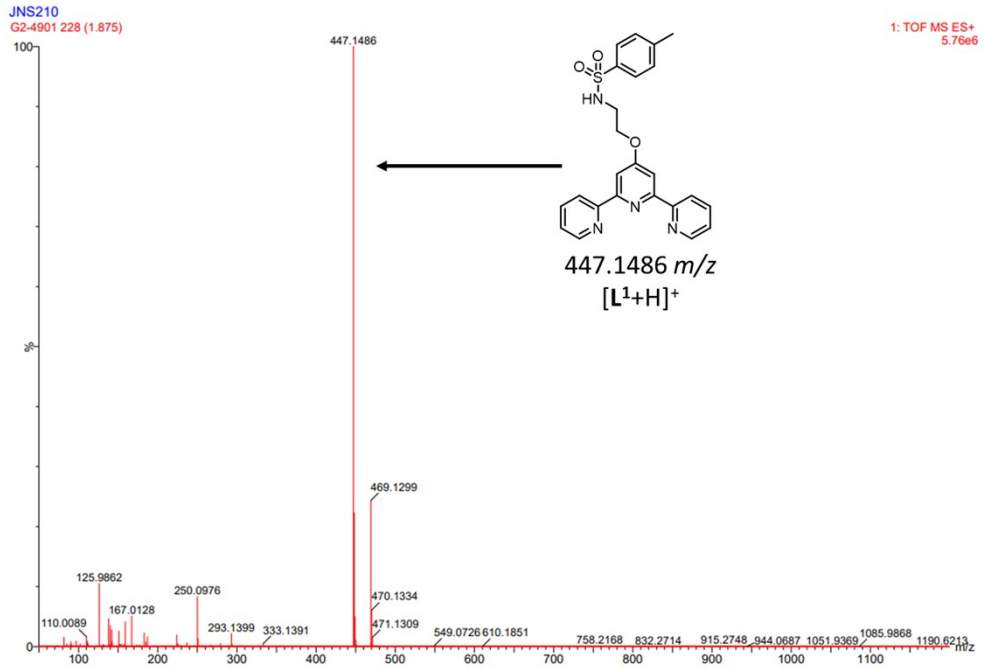

Figure S18. High-resolution ESI-MS mass spectrum (positive mode) of **L**[1].

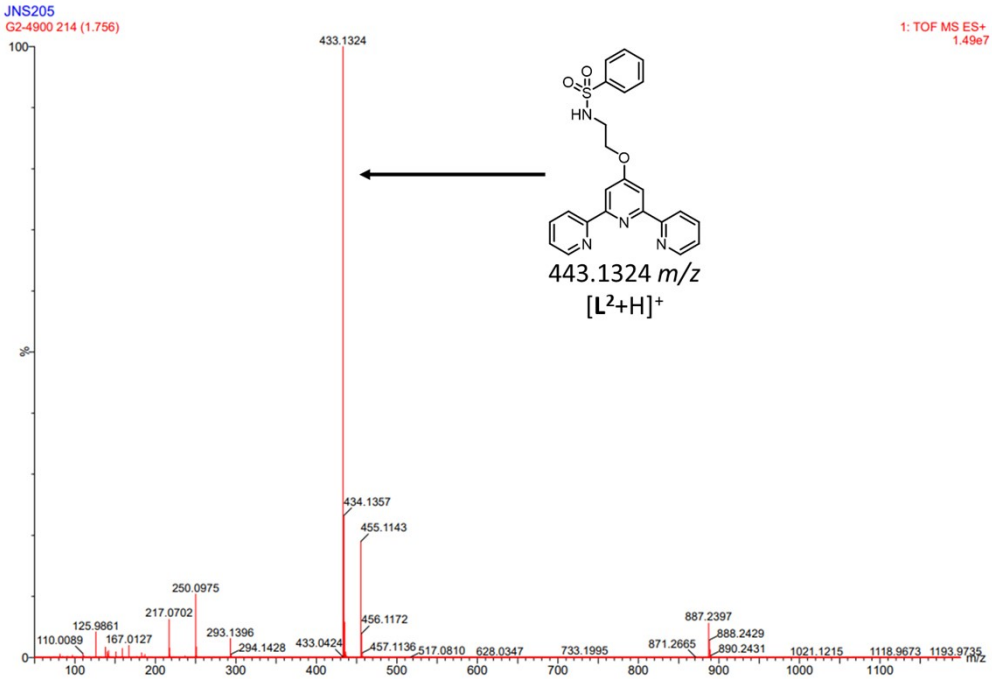

Figure S19. High-resolution ESI-MS mass spectrum (positive mode) of **L**[2].

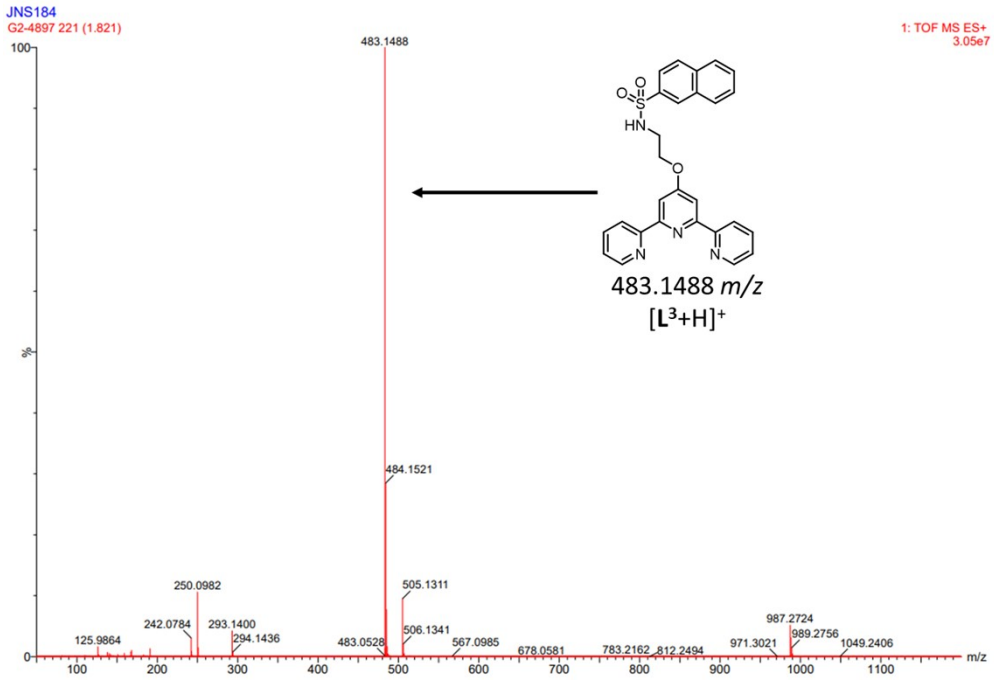

Figure S20. High-resolution ESI-MS mass spectrum (positive mode) of **L**^{3}.

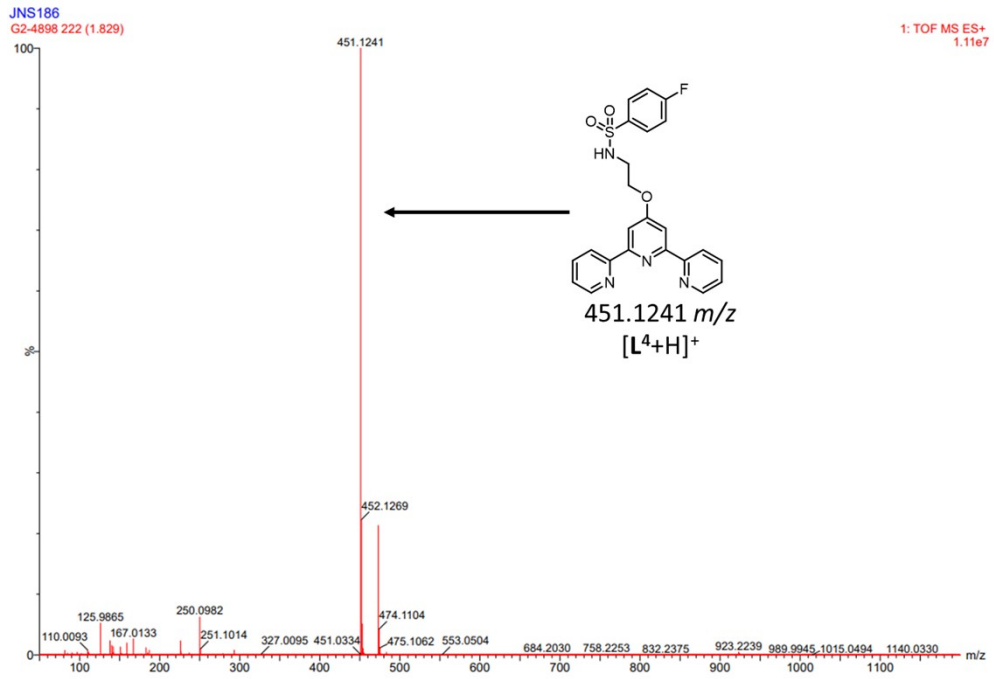

Figure S21. High-resolution ESI-MS mass spectrum (positive mode) of **L**^{4}.

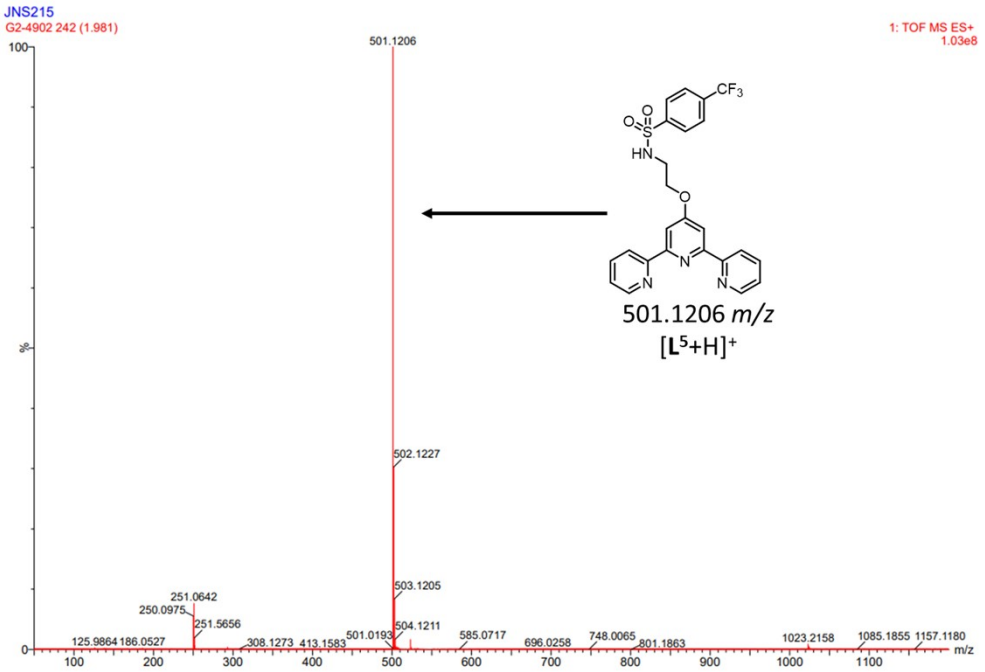

Figure S22. High-resolution ESI-MS mass spectrum (positive mode) of $\mathbf{L^5}$.

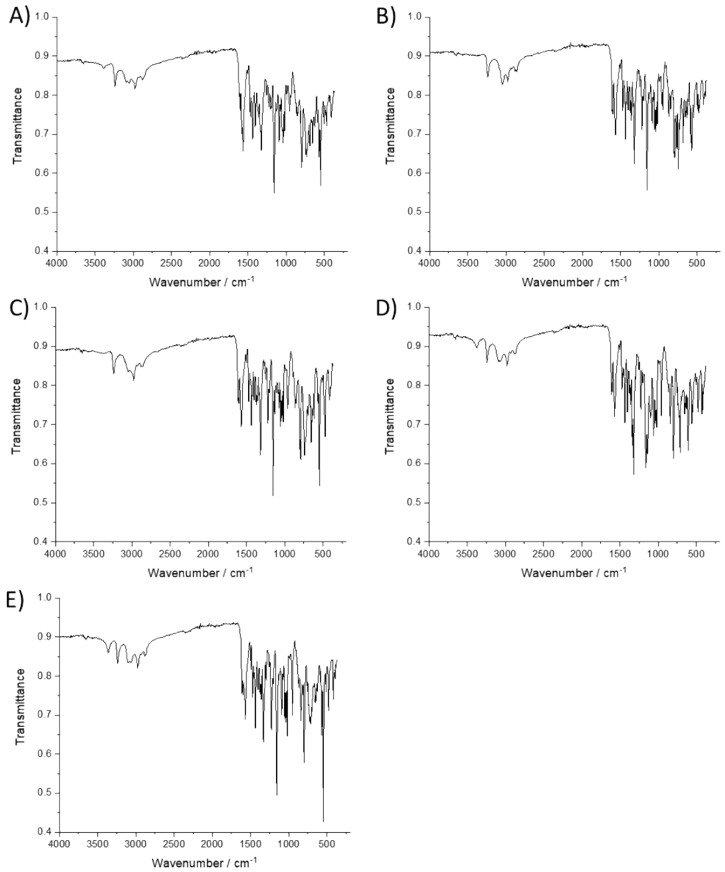

Figure S23. ATR-FTIR spectra of (A) **1**, (B) **2**, (C) **3**, (D) **4**, (E) **5** in the solid form.

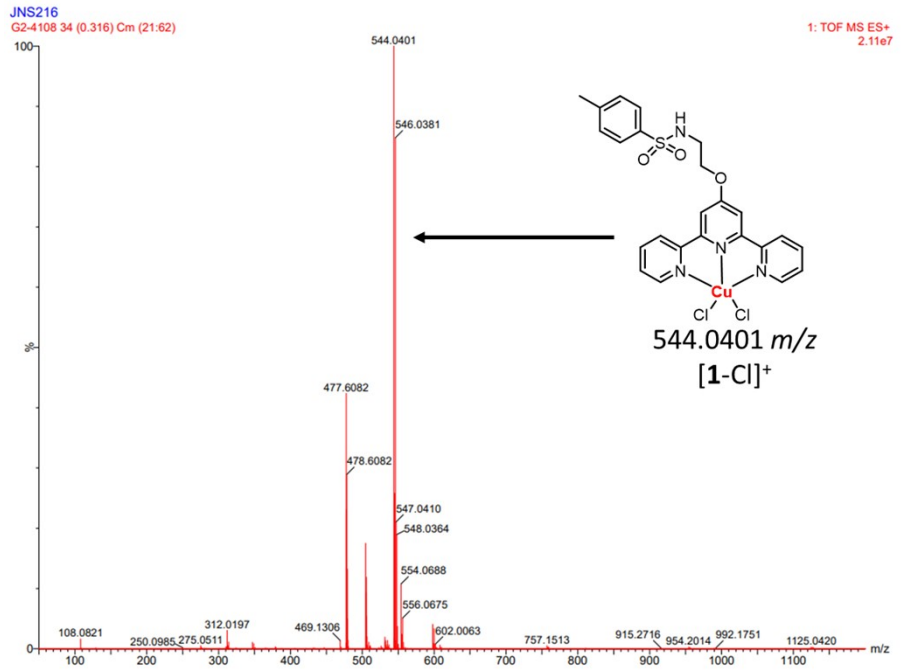

Figure S24. High-resolution ESI-MS mass spectrum (positive mode) of **1**.

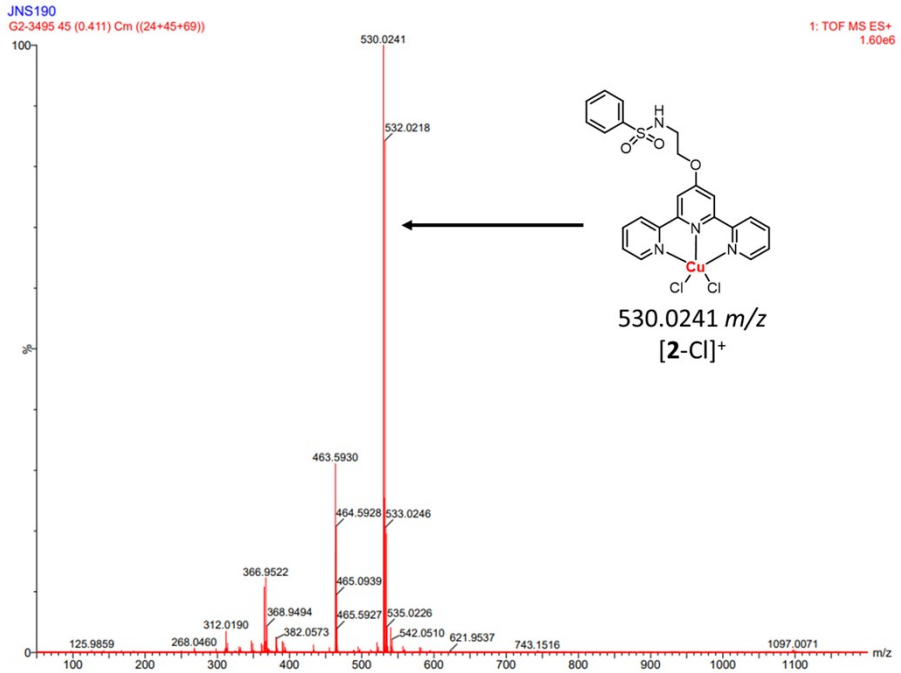

Figure S25. High-resolution ESI-MS mass spectrum (positive mode) of **2**.

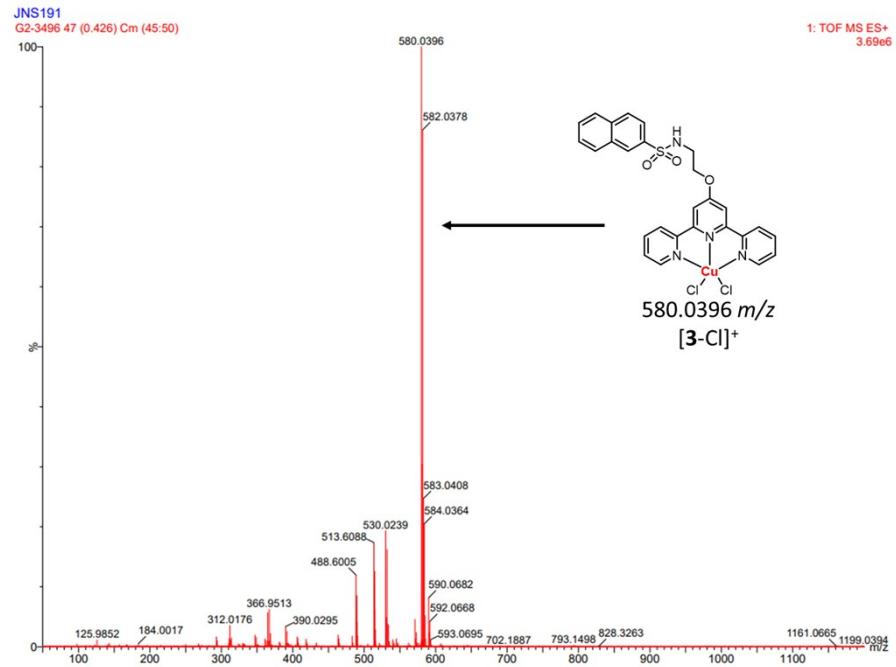

Figure S26. High-resolution ESI-MS mass spectrum (positive mode) of **3**.

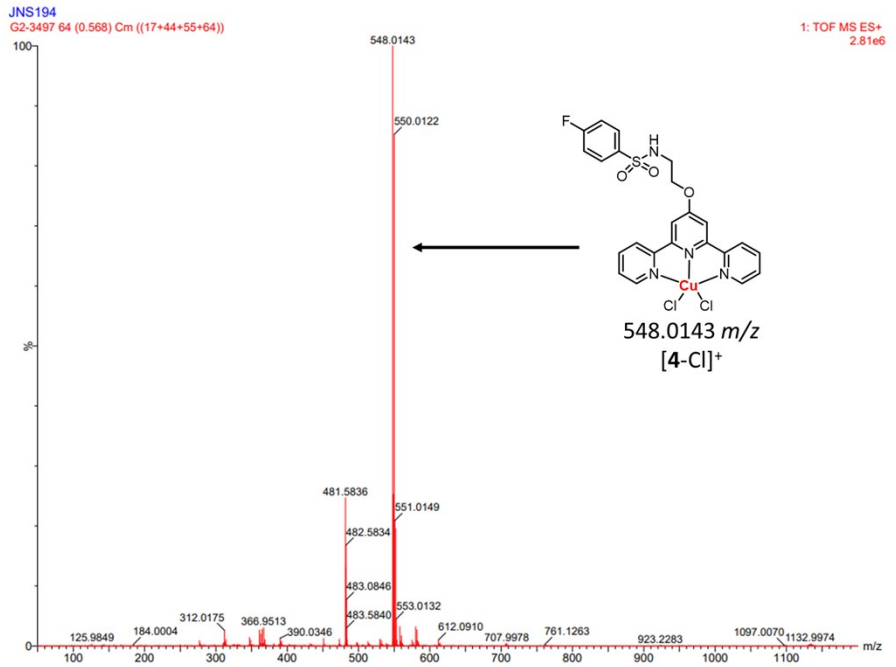

Figure S27. High-resolution ESI-MS mass spectrum (positive mode) of **4**.

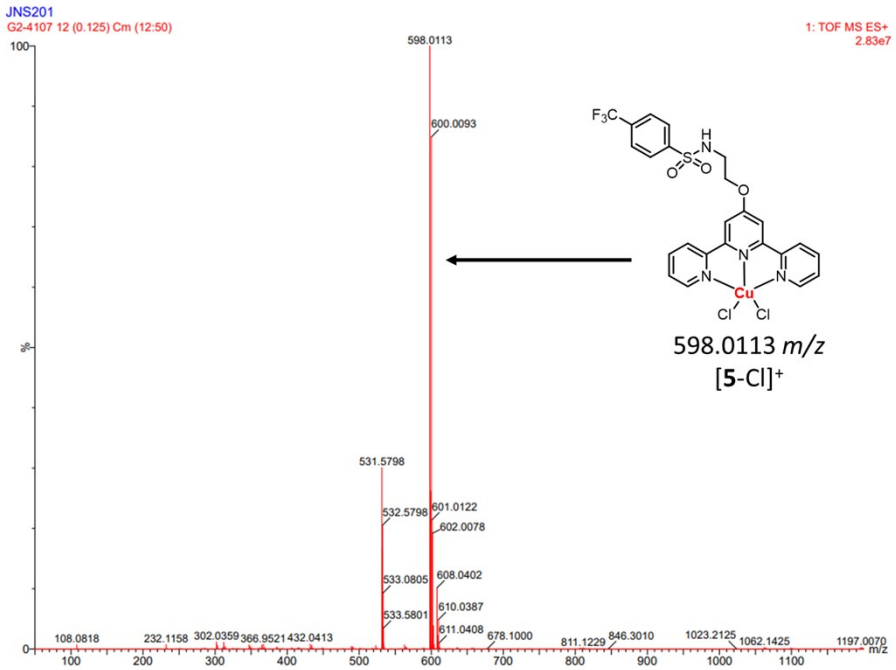

Figure S28. High-resolution ESI-MS mass spectrum (positive mode) of **5**.

Table S1. Crystallographic data for complexes **1**-**3**.

Metal complex	**1**	**2**	**3**
CCDC No.	2258101	2258099	2258098
formula	$C_{24}H_{22}Cl_2CuN_4O_3S$	$C_{23}H_{20}Cl_2CuN_4O_3S$	$C_{27}H_{22}Cl_2CuN_4O_3S + CH_3CN$
Fw	580.95	566.93	658.04
Crystal system	triclinic	orthorhombic	triclinic
Space group	P-1	Pbca	P-1
a, Å	7.7408(5)	14.013(3)	7.7290(2)
b, Å	8.5955(6)	13.767(3)	8.4595(2)
c, Å	19.5113(13)	24.041(5)	23.7162(7)
α, deg.	86.001(3)	90	80.9710(10)
β, deg.	78.691(3)	90	83.8520(10)
γ, deg.	72.651(3)	90	69.4890(10)
V, Å^3	1215.00(14)	4638.0(18)	1432.07(7)
Z	2	8	2
D_{calcd}, Mg/m^3	1.588	1.624	1.526
2*θ* / deg.	4.618 to 133.532	1.69 to 26.00	7.56 to 144.46
Reflections collected	28912	34260	45499
Independent reflections	4295	4558	5648
Goodness-of-fit on F^2	1.077	0.949	1.052
R_1, wR_2 [$I \geq 2\sigma(I)$]	0.0492, 0.1448	0.0419, 0.0909	0.0330, 0.0898
R_1, wR_2 [all data]	0.0518, 0.1476	0.0622, 0.0967	0.0333, 0.0901

Table S2. Crystallographic data for complexes **4**-**5**.

Metal complex	**4**	**5**
CCDC No.	2258097	2258100
formula	$2\times(C_{23}H_{19}Cl_2CuFN_4O_3S) + 1.5H_2O$	$C_{24}H_{19}Cl_2CuF_3N_4O_3S + CH_3CN$
Fw	1196.87	675.98
Crystal system	triclinic	triclinic
Space group	P-1	P-1
a, Å	8.1461(6)	8.3057(6)
b, Å	8.5293(7)	8.5238(6)
c, Å	19.2202(16)	20.6586(14)
α, deg.	88.390(3)	87.401(2)
β, deg.	78.390(3)	80.917(2)
γ, deg.	72.100(3)	71.980(2)
V, Å^3	1243.97(17)	1373.36(17)
Z	1	2
D_{calcd}, Mg/m^3	1.598	1.635
2*θ* / deg.	4.696 to 110.08	4.332 to 144.638
Reflections collected	14856	20455
Independent reflections	3111	5383
Goodness-of-fit on F^2	1.037	1.118
R_1, wR_2 [$I\geq2\sigma(I)$]	0.0631, 0.1592	0.0540, 0.1460
R_1, wR_2 [all data]	0.0720, 0.1712	0.0562, 0.1480

Table S3. Selected bond lengths (Å) for complexes **1**-**5**.

Bond	**1**	**2**	**3**	**4**	**5**
Cu(1)-N(2)	1.942(2)	1.957(3)	1.9364 (14)	1.941(4)	1.940(3)
Cu(1)-N(3)	2.033(2)	2.047(3)	2.0304 (15)	2.046(4)	2.048(3)
Cu(1)-N(1)	2.032(2)	2.053(3)	2.0294 (15)	2.035(4)	2.044(3)
Cu(1)-Cl(1)	2.2352(7)	2.2428(9)	2.2344(5)	2.2366(14)	2.2348(9)
Cu(1)-Cl(2)	2.6405(8)	2.4525(10)	2.7519(5)	2.6012(15)	2.5643(9)

Table S4. Selected bond angles (°) for complexes **1**-**5**.

Bond angle	**1**	**2**	**3**	**4**	**5**
N(2)-Cu(1)-N(3)	79.99(9)	78.99(10)	79.61(6)	79.99(16)	79.24(11)
N(2)-Cu(1)-N(1)	79.63(9)	78.75(10)	80.28(6)	79.56(16)	79.71(11)
N(3)-Cu(1)-N(1)	158.98(10)	155.16(10)	159.58(6)	159.01(16)	157.95(11)
N(2)-Cu(1)-Cl(1)	169.64(7)	162.51(8)	172.37(5)	169.19(13)	167.08(8)
N(3)-Cu(1)-Cl(1)	99.25(7)	98.92(8)	100.33(4)	99.52(12)	99.70(8)
N(1)-Cu(1)-Cl(1)	99.87(7)	98.99(8)	99.13(4)	99.67(13)	99.33(8)
N(2)-Cu(1)-Cl(2)	83.78(7)	94.63(8)	79.65(4)	87.10(12)	89.39(8)
N(3)-Cu(1)-Cl(2)	92.60(7)	93.55(7)	87.51(4)	92.91(12)	91.63(8)
N(1)-Cu(1)-Cl(2)	90.24(7)	99.08(7)	92.37(4)	90.76(12)	94.64(8)
Cl(1)-Cu(1)-Cl(2)	106.59(3)	102.84(3)	107.97(18)	103.70(5)	103.52(3)

Table S5. Experimentally determined LogP values for copper(II)-terpyridine complexes **1-5** and Cu(2,2';6',2"-terpyridine)Cl_2.

Copper(II)-terpyridine complex	LogP value
1	-1.83 ± 0.09
2	-1.96 ± 0.03
3	-1.71 ± 0.08
4	-2.18 ± 0.16
5	-2.27 ± 0.04
Cu(terpy)Cl_2	-2.01 ± 0.08

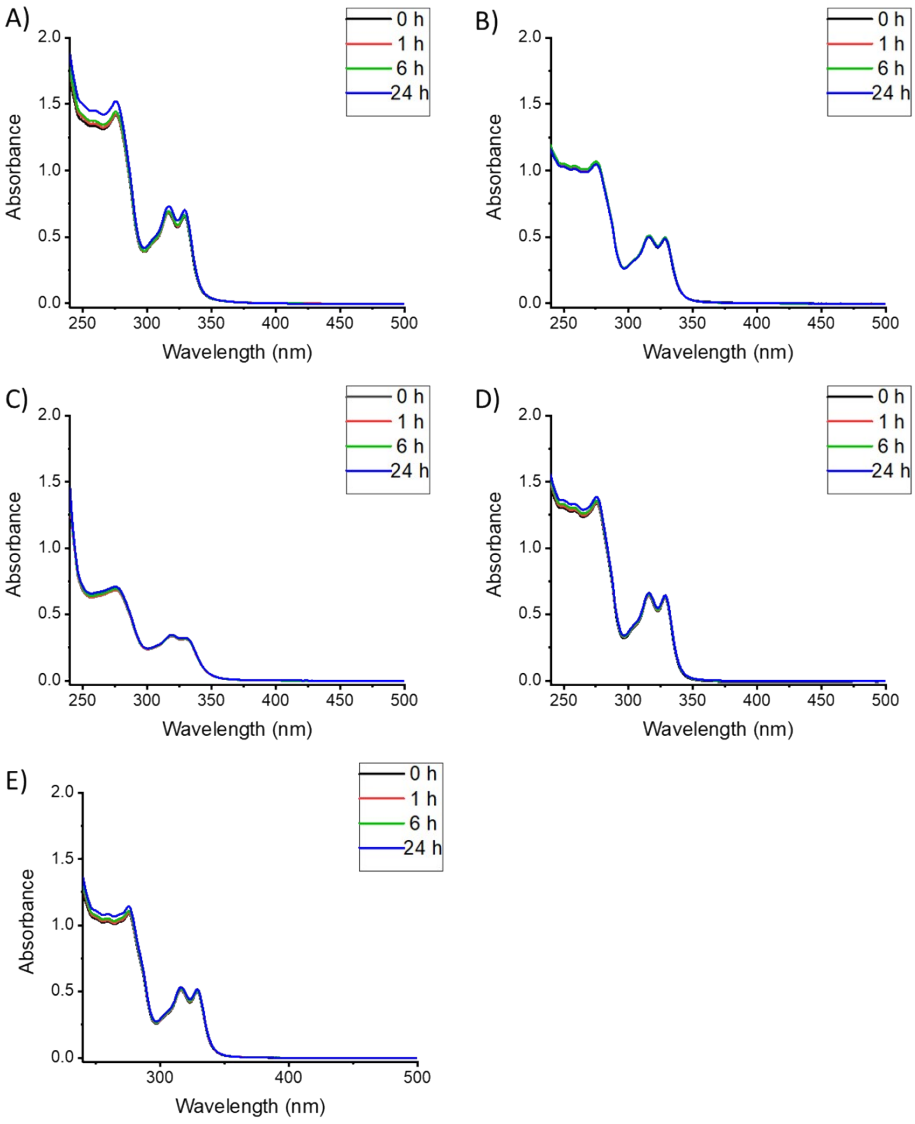

Figure S29. UV-Vis spectra of **1-5** (A-E) (all 50 µM) in PBS:DMSO (200:1) over the course of 24 h at 37 °C.

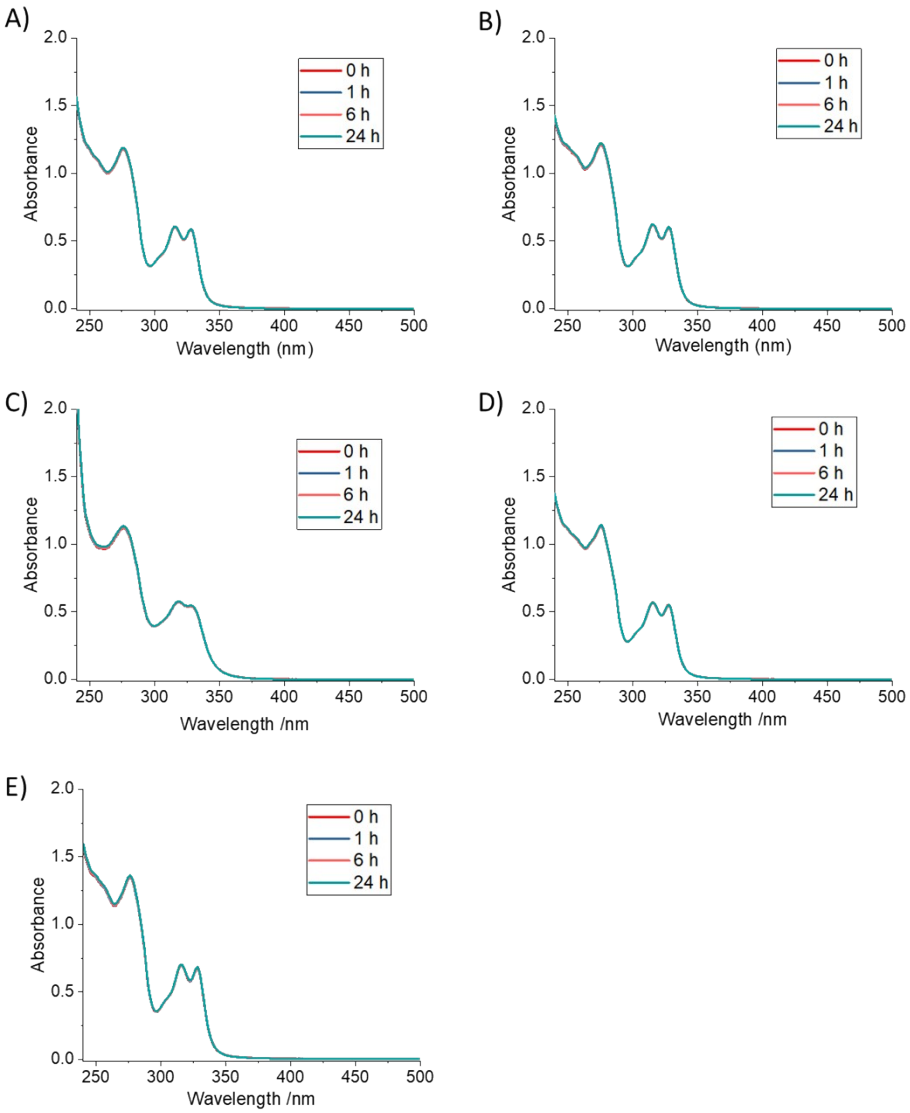

Figure S30. UV-Vis spectra of **1-5** (A-E) (all 50 µM) in H_2O:DMSO (200:1) over the course of 24 h at 37 °C.

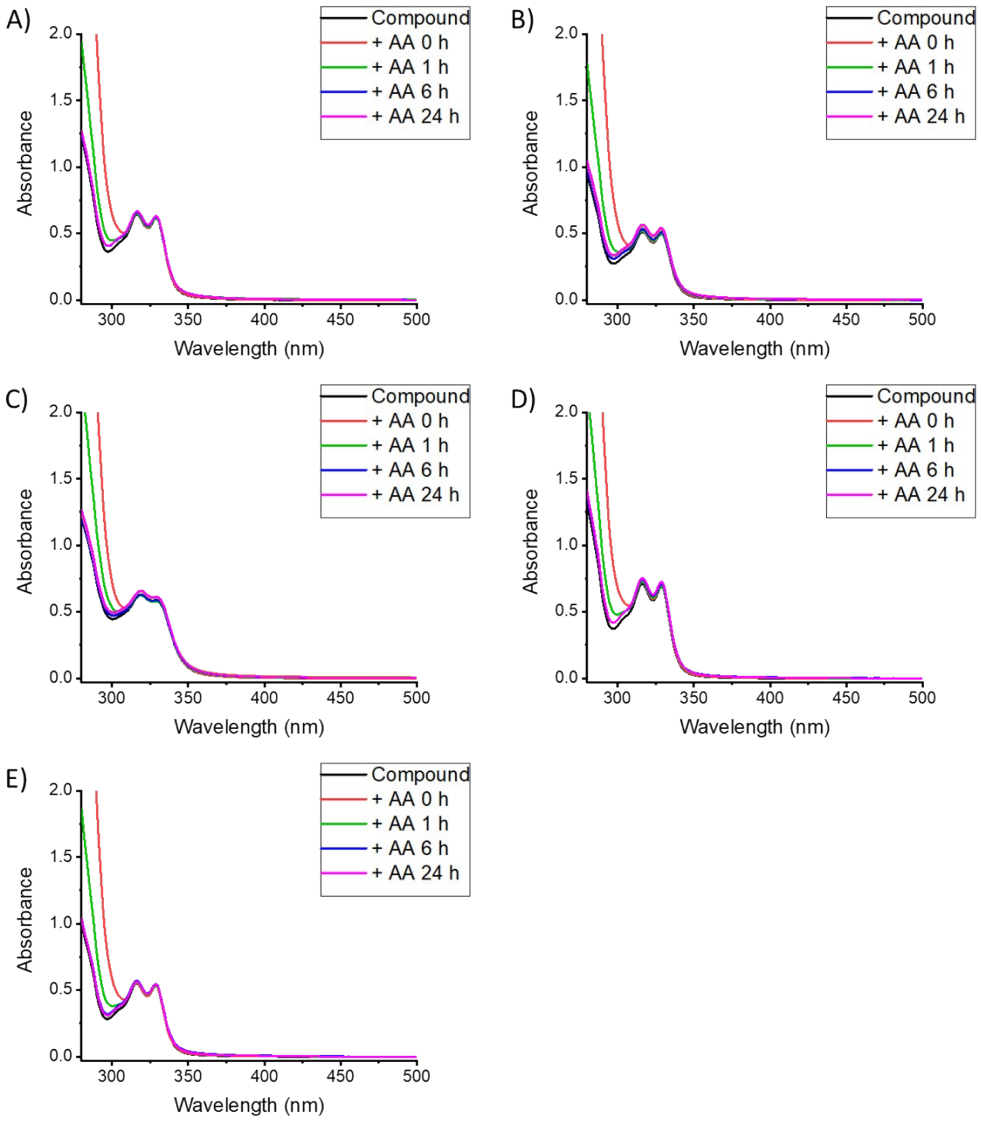

Figure S31. UV-Vis spectra of **1-5** (A-E) (all 50 µM) in PBS:DMSO (200:1) in the presence of ascorbic acid (0.5 mM) over the course of 24 h at 37 °C.

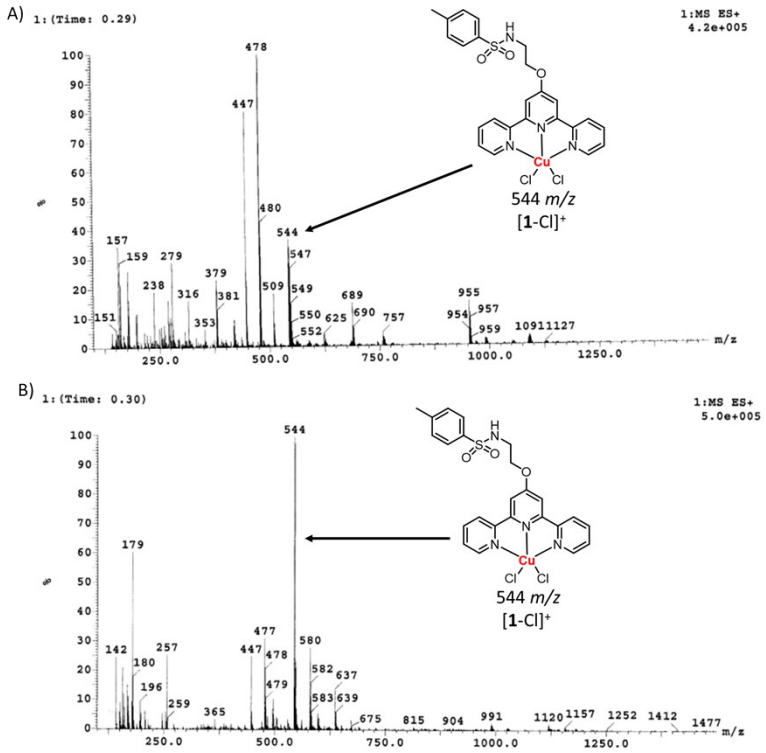

Figure S32. ESI mass spectra (positive mode) of **1** (500 μM) in H_2O:DMSO (5:1) in the presence of (A) ascorbic acid (5 mM) or (B) glutathione (5 mM) after incubation for 24 h at 37 ^oC.

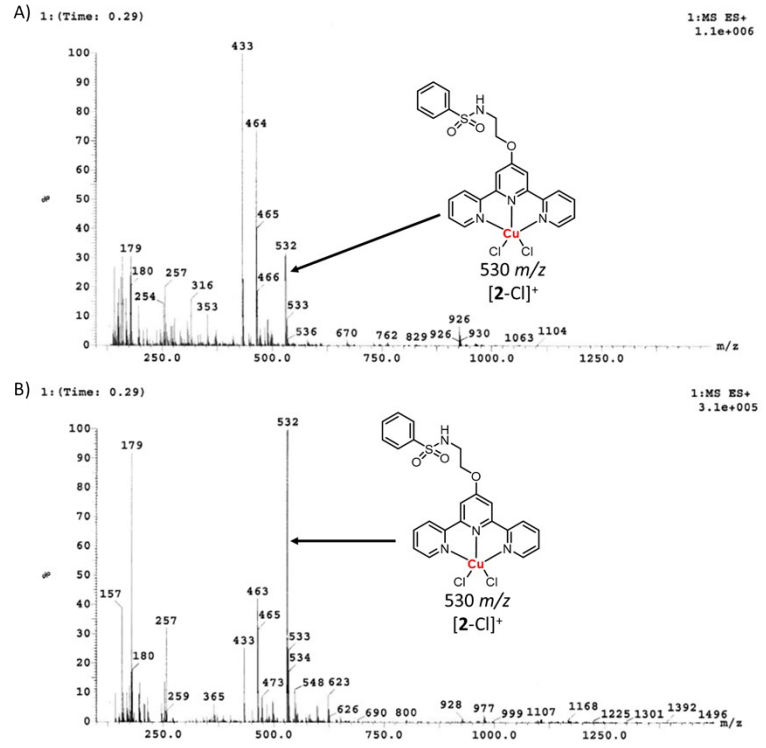

Figure S33. ESI mass spectra (positive mode) of **2** (500 μM) in H_2O:DMSO (5:1) in the presence of (A) ascorbic acid (5 mM) or (B) glutathione (5 mM) after incubation for 24 h at 37 ^oC.

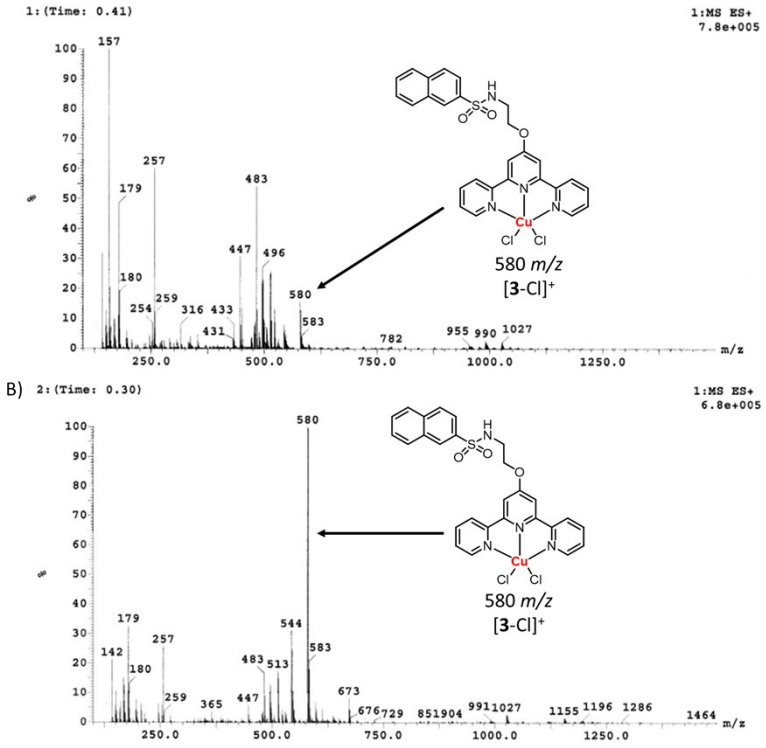

Figure S34. ESI mass spectra (positive mode) of **3** (500 μM) in H_2O:DMSO (5:1) in the presence of (A) ascorbic acid (5 mM) or (B) glutathione (5 mM) after incubation for 24 h at 37 ^oC.

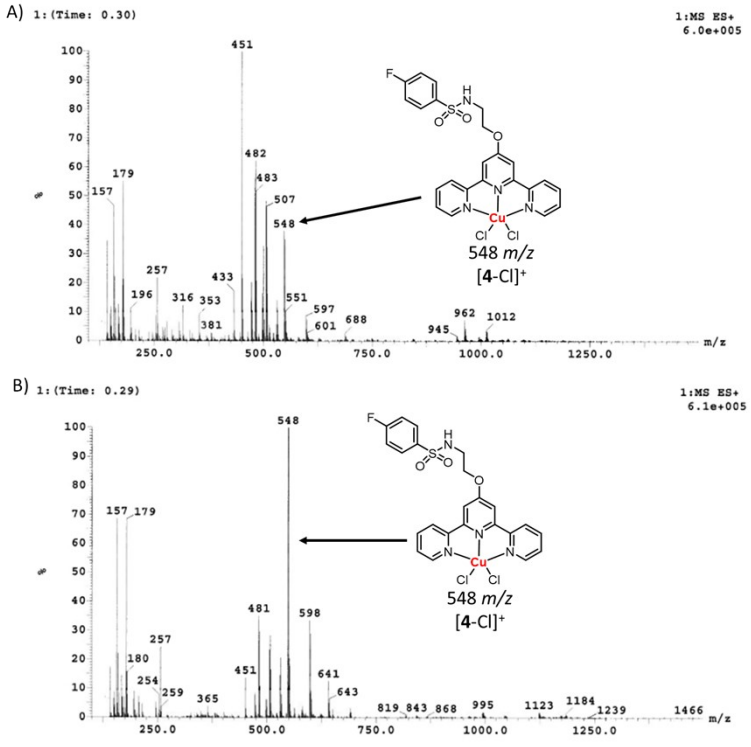

Figure S35. ESI mass spectra (positive mode) of **4** (500 μM) in H_2O:DMSO (5:1) in the presence of (A) ascorbic acid (5 mM) or (B) glutathione (5 mM) after incubation for 24 h at 37 ^oC.

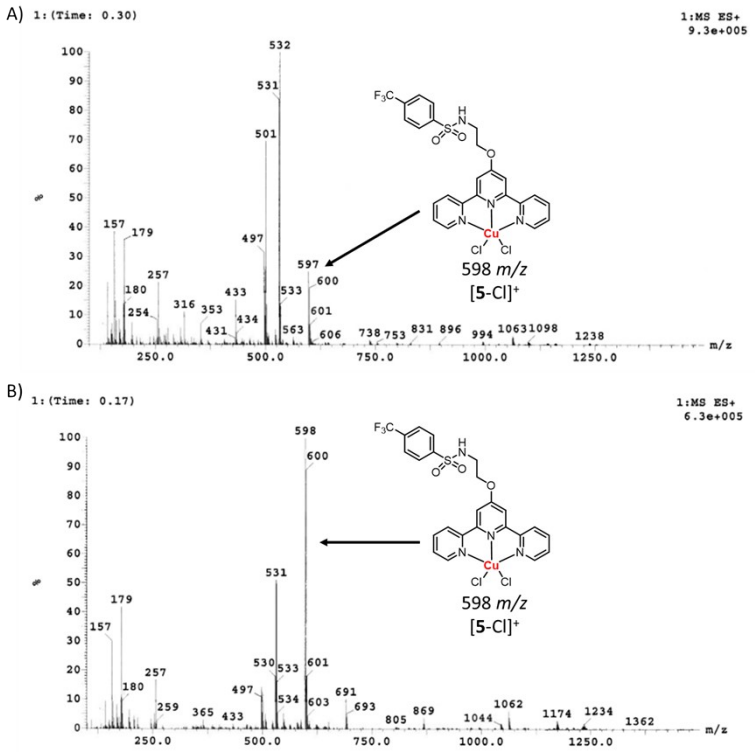

Figure S36. ESI mass spectra (positive mode) of **5** (500 μM) in H_2O:DMSO (5:1) in the presence of (A) ascorbic acid (5 mM) or (B) glutathione (5 mM) after incubation for 24 h at 37 ^oC.

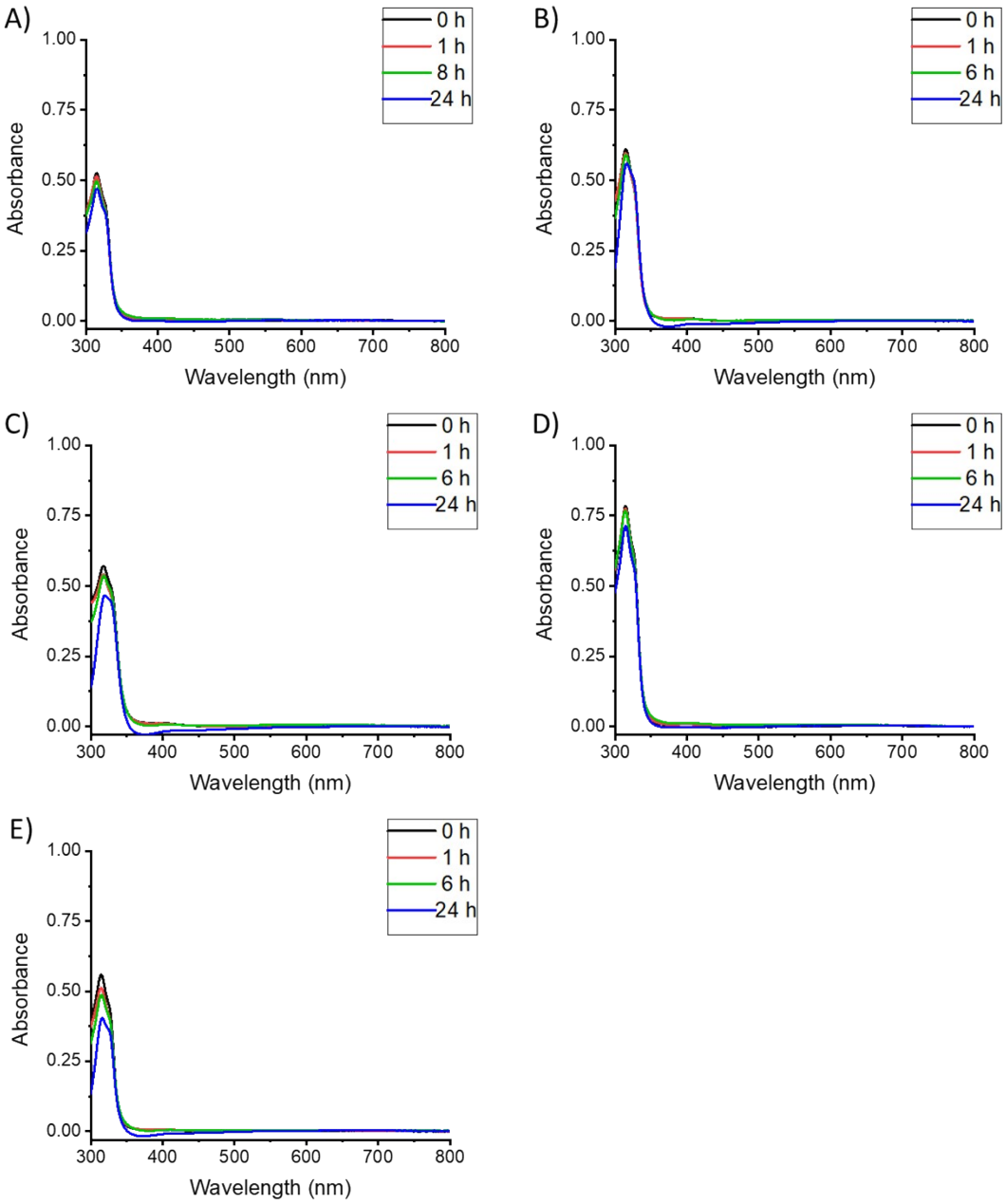

Figure S37. UV-Vis spectra of **1-5** (A-E) (all 50 μM) in Mammary Epithelial Cell Growth Medium (MEGM):DMSO (200:1) over the course of 24 h at 37 °C.

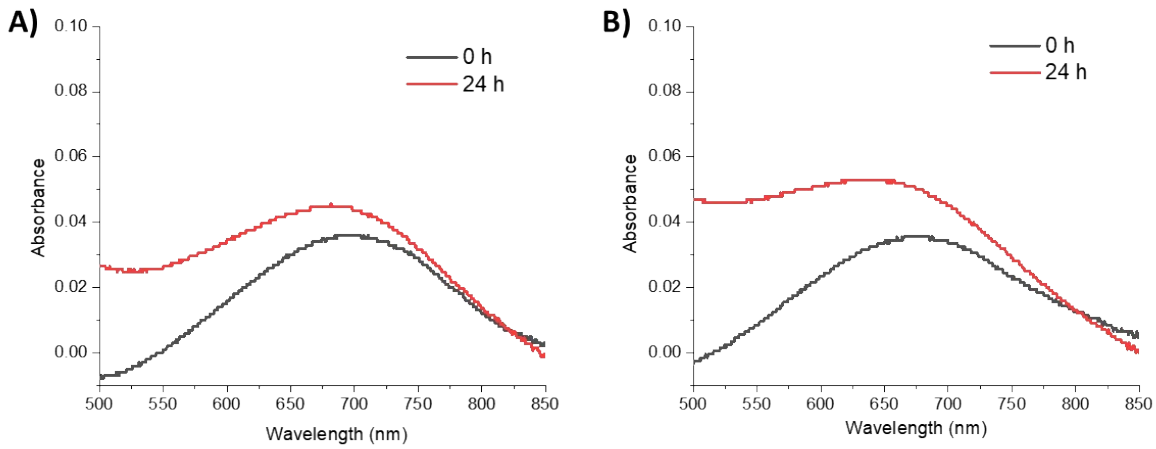

Figure S38. UV-Vis spectra of **1** (0.5 mM) in (A) PBS:DMSO (10:1) and (B) Mammary Epithelial Cell Growth Medium (MEGM):DMSO (10:1) before and after incubation at 37 °C for 24 h.

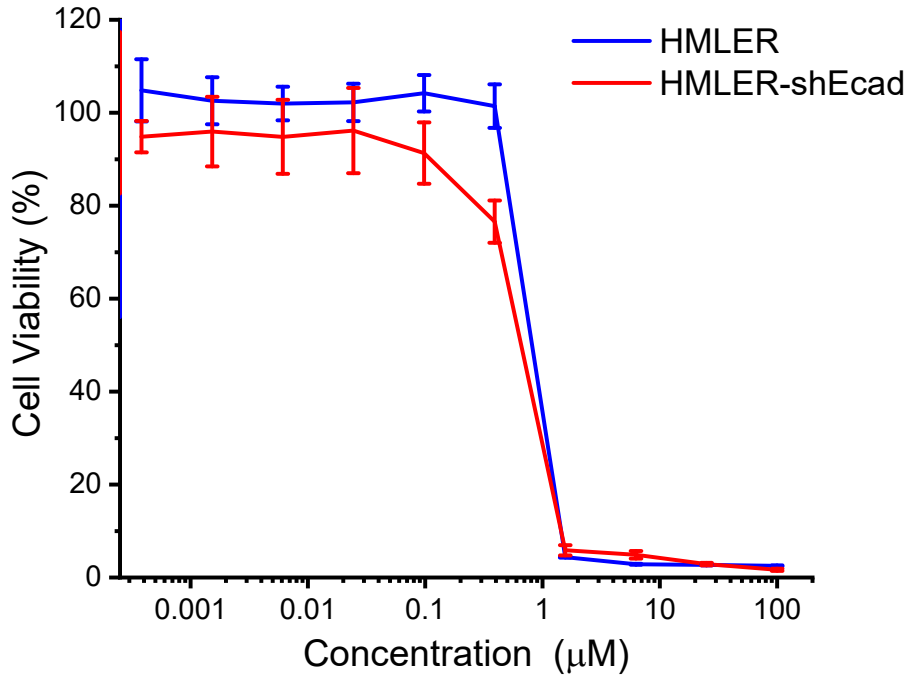

Figure S39. Representative dose-response curves for the treatment of HMLER and HMLER-shEcad cells with **1** after 72 h incubation.

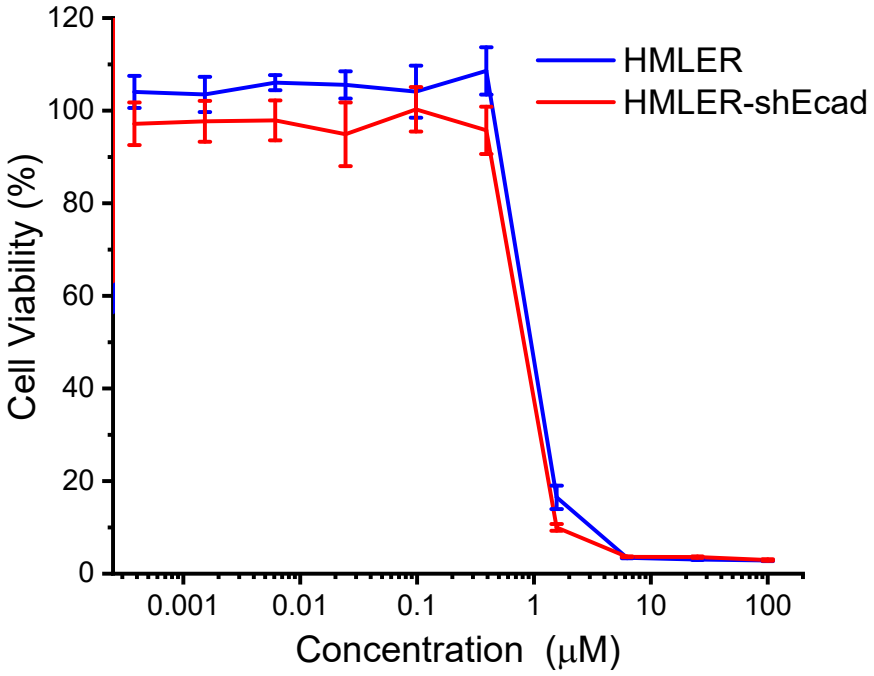

Figure S40. Representative dose-response curves for the treatment of HMLER and HMLER-shEcad cells with **2** after 72 h incubation.

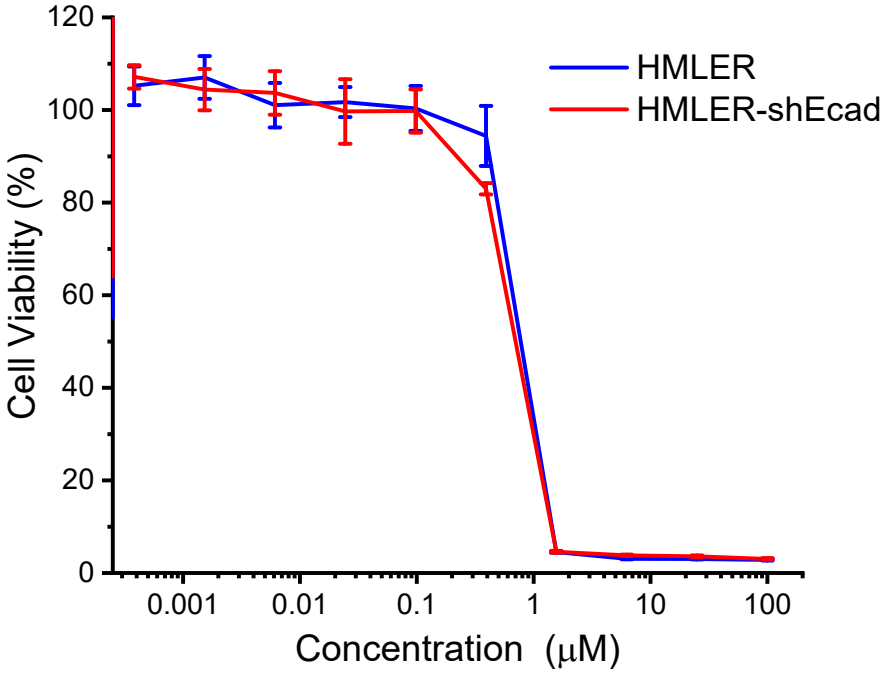

Figure S41. Representative dose-response curves for the treatment of HMLER and HMLER-shEcad cells with **3** after 72 h incubation.

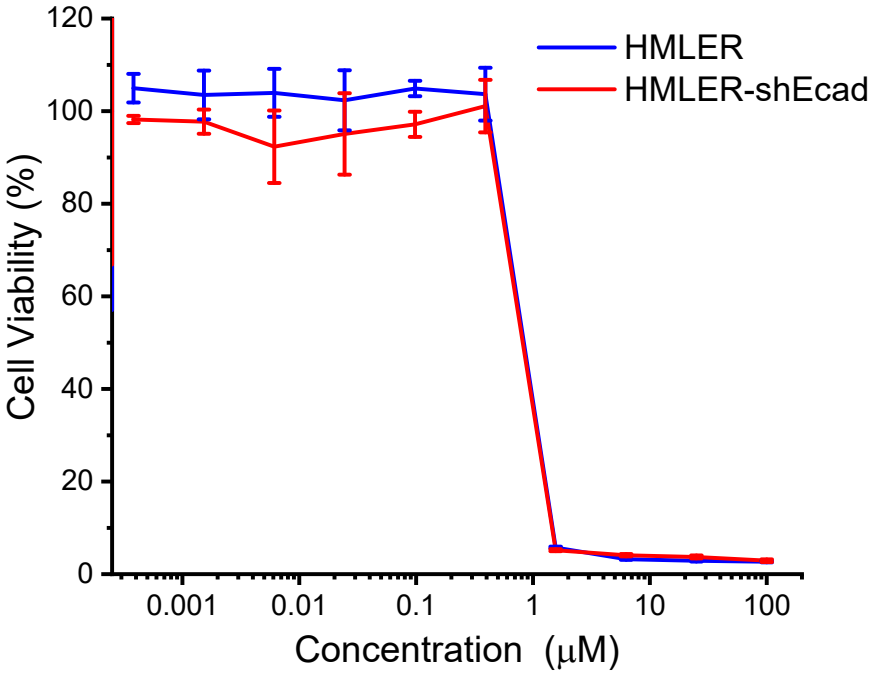

Figure S42. Representative dose-response curves for the treatment of HMLER and HMLER-shEcad cells with **4** after 72 h incubation.

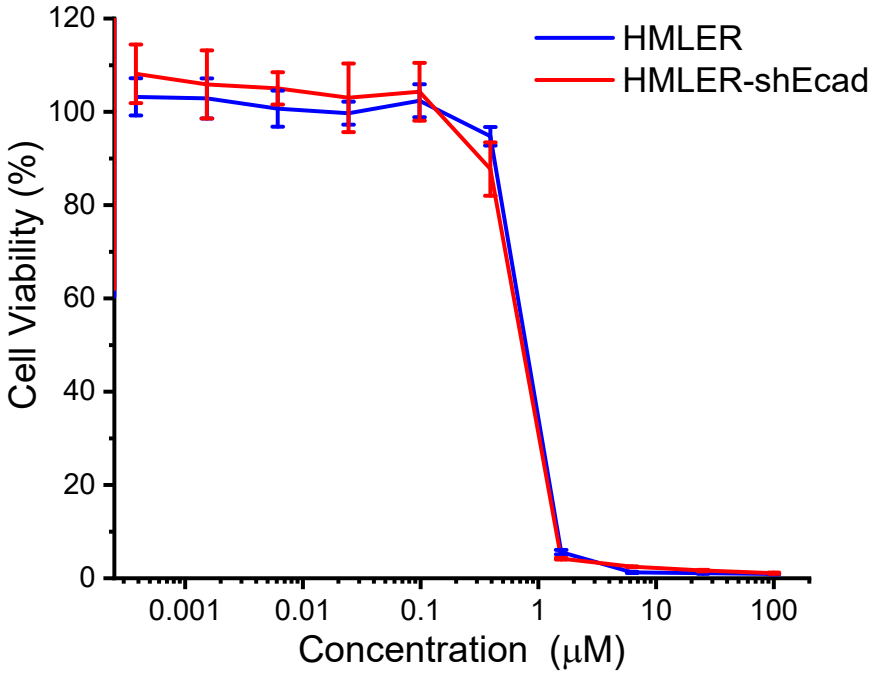

Figure S43. Representative dose-response curves for the treatment of HMLER and HMLER-shEcad cells with **5** after 72 h incubation.

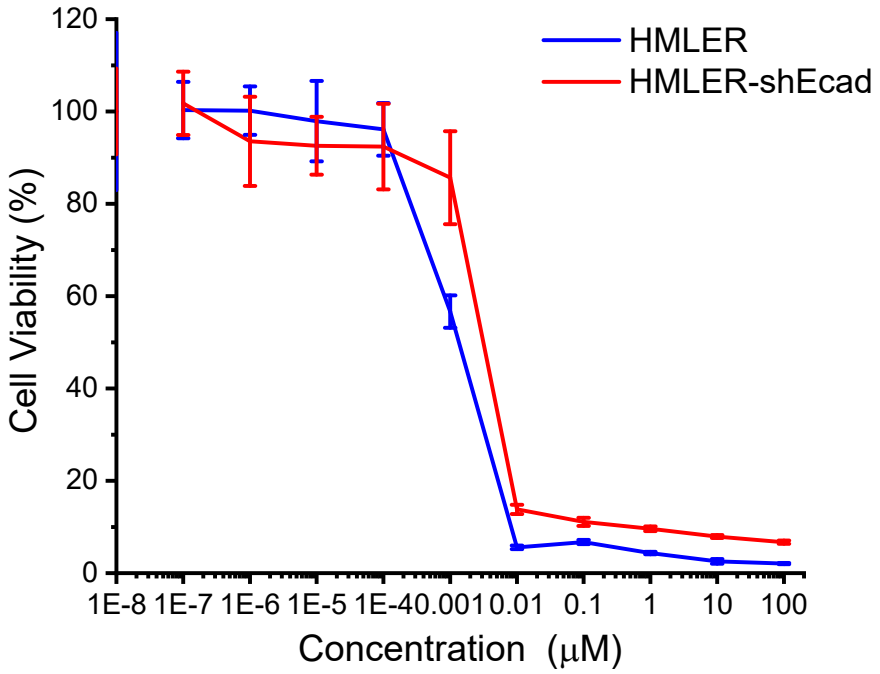

Figure S44. Representative dose-response curves for the treatment of HMLER and HMLER-shEcad cells with gemcitabine after 72 h incubation.

Table S6. IC_{50} values of the gemcitabine, 5-fluorouracil, capecitabine, and carboplatin against HMLER and HMLER-shEcad cells. [a] Determined after 72 h incubation (mean of three independent experiments ± SD). [b] Reported in reference [1].

Compound	HMLER [μM] [a]	HMLER-shEcad [μM] [a]
gemcitabine	0.0014 ± 0.0002	0.0031 ± 0.0003
5-fluorouracil [b]	41.05 ± 5.30	49.10 ± 5.94
capecitabine [b]	> 100	> 100
carboplatin [b]	67.31 ± 2.80	72.39 ± 7.99

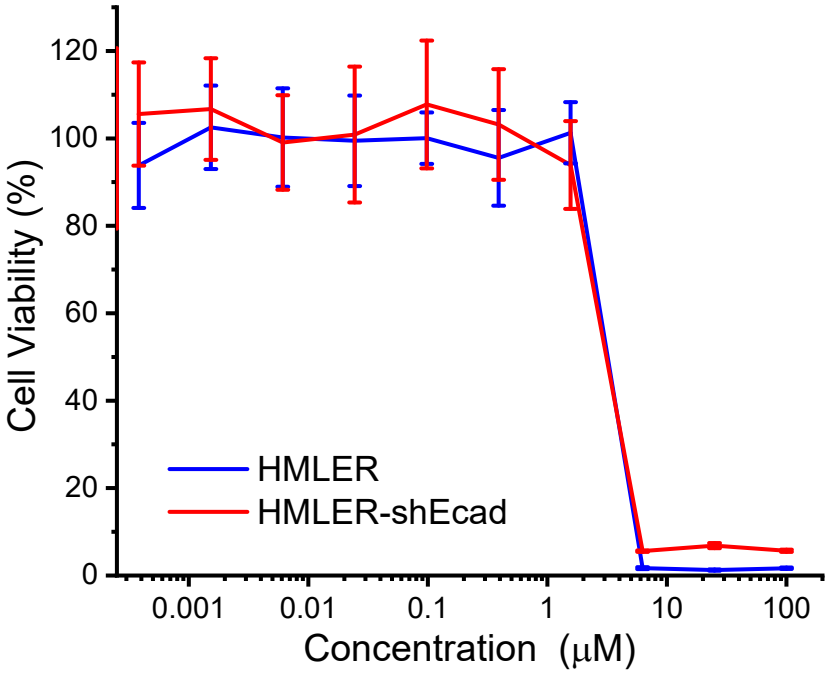

Figure S45. Representative dose-response curves for the treatment of HMLER and HMLER-shEcad cells with **L**[1] after 72 h incubation.

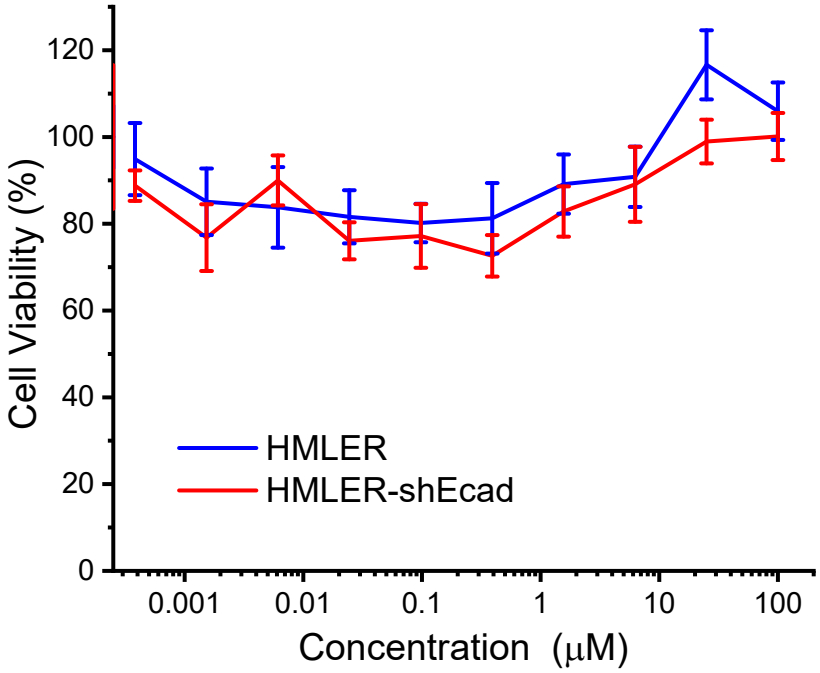

Figure S46. Representative dose-response curves for the treatment of HMLER and HMLER-shEcad cells with copper nitrate after 72 h incubation.

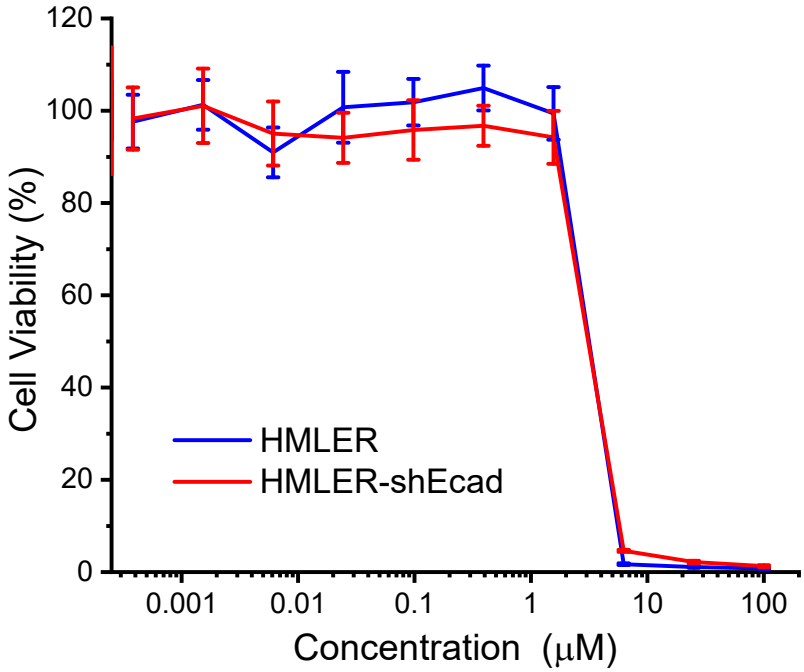

Figure S47. Representative dose-response curves for the treatment of HMLER and HMLER-shEcad cells with Cu(2,2';6',2"-terpyridine)Cl_2 after 72 h incubation.

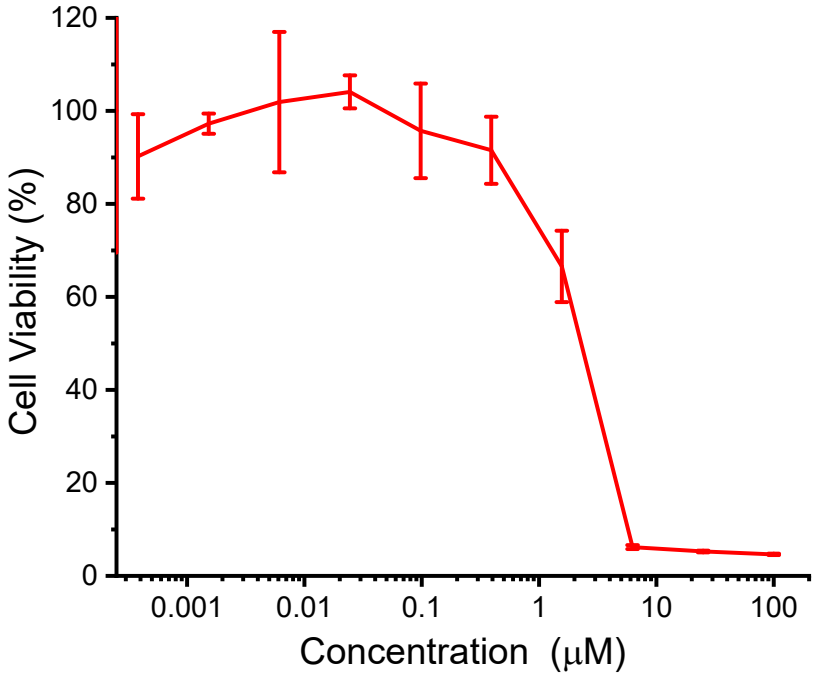

Figure S48. Representative dose-response curves for the treatment of HMLER-shEcad cells with $\mathbf{L^1}$ + $CuCl_2$ (1:1) after 72 h incubation.

Figure S49. Representative bright-field images (× 10) of HMLER-shEcad spheroids in the absence and presence of salinomycin or cisplatin at their IC_{20} value (5 days incubation).

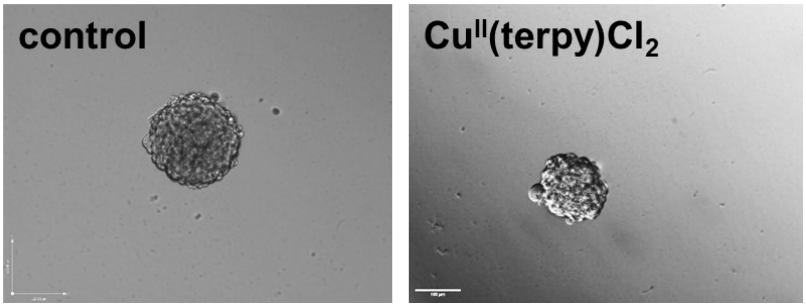

Figure S50. Representative bright-field images (× 10) of HMLER-shEcad spheroids in the absence and presence of Cu(2,2';6',2"-terpyridine)Cl_2 at its IC_{20} value (5 days incubation).

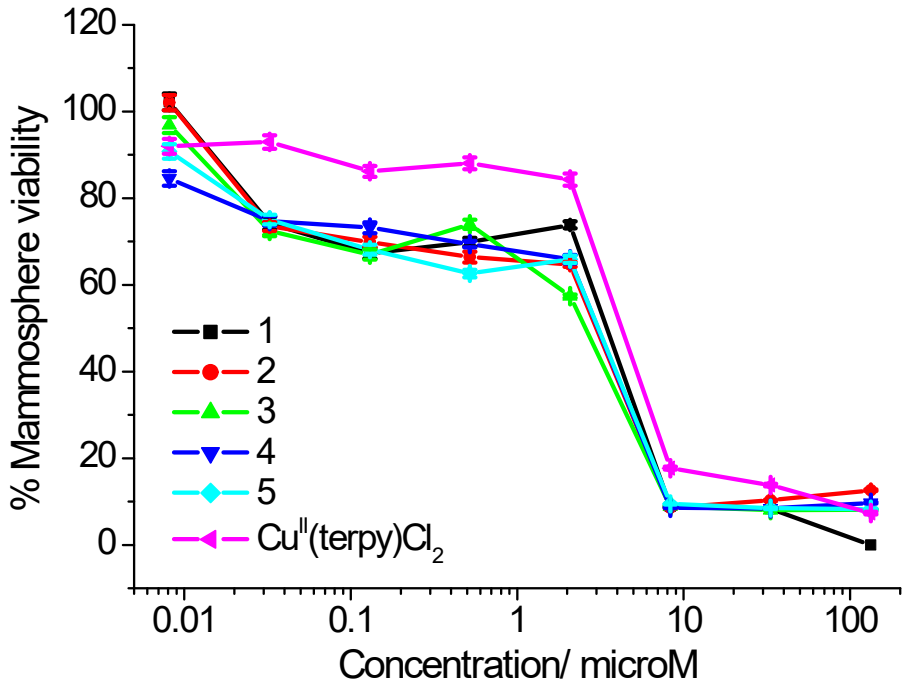

Figure S51. Representative dose-response curves for the treatment of HMLER-shEcad mammospheres with **1**-**5** or Cu(2,2';6',2"-terpyridine)Cl_2 after 5 days incubation. Error bars = SD.

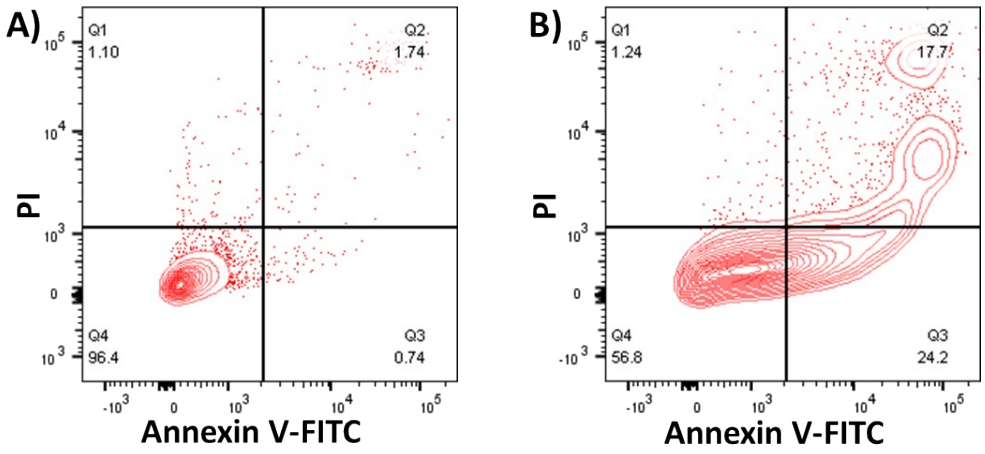

Figure S52. FITC Annexin V-propidium iodide binding assay plots of (A) untreated HMLER-shEcad cells and (B) HMLER-shEcad cells treated with cisplatin (25 μM for 48 h).

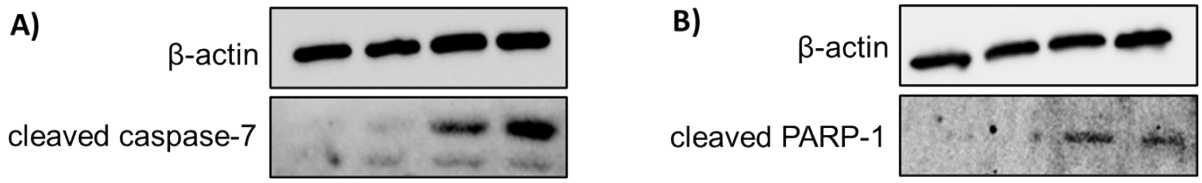

Figure S53. Immunoblotting analysis of proteins related to the apoptosis pathway. Protein expression in HMLER-shEcad cells untreated and treated with (A) **1** (0.4, 0.8, and 1.6 μM for 24 h) or (B) **1** (0.4, 0.8, and 1.6 μM for 48 h).

Reference

1. A. Johnson, C. Olelewe, J. H. Kim, J. Northcote-Smith, R. T. Mertens, G. Passeri, K. Singh, S. G. Awuah and K. Suntharalingam, *Chem. Sci.*, 2023, **14**, 557-565.